AFRL-AFOSR-JP-TR-2016-0084

Novel techniques for quantification of correlation between primary liquid jet breakup and downstream spray characteristics

Yannis Hardalupas
IMPERIAL COLLEGE OF SCIENCE TECHNOLOGY & MEDICINE

10/05/2016
Final Report

Air Force Research Laboratory
AF Office Of Scientific Research (AFOSR)/ IOA
Arlington, Virginia 22203
Air Force Materiel Command

REPORT DOCUMENTATION PAGE

Form Approved
OMB No. 0704-0188

1. REPORT DATE *(DD-MM-YYYY)*	2. REPORT TYPE	3. DATES COVERED *(From - To)*
17-10-2016	Final	18 Apr 2013 to 17 Apr 2016

4. TITLE AND SUBTITLE
Novel techniques for quantification of correlation between primary liquid jet breakup and downstream spray characteristics

5a. CONTRACT NUMBER

5b. GRANT NUMBER
FA2386-13-1-4065

5c. PROGRAM ELEMENT NUMBER
61102F

6. AUTHOR(S)
Yannis Hardalupas

5d. PROJECT NUMBER

5e. TASK NUMBER

5f. WORK UNIT NUMBER

7. PERFORMING ORGANIZATION NAME(S) AND ADDRESS(ES)
IMPERIAL COLLEGE OF SCIENCE TECHNOLOGY & MEDICINE
EXHIBITION RD
LONDON, SW7 2BT GB

8. PERFORMING ORGANIZATION REPORT NUMBER

9. SPONSORING/MONITORING AGENCY NAME(S) AND ADDRESS(ES)
AOARD
UNIT 45002
APO AP 96338-5002

10. SPONSOR/MONITOR'S ACRONYM(S)
AFRL/AFOSR IOA

11. SPONSOR/MONITOR'S REPORT NUMBER(S)
AFRL-AFOSR-JP-TR-2016-0084

12. DISTRIBUTION/AVAILABILITY STATEMENT
A DISTRIBUTION UNLIMITED: PB Public Release

13. SUPPLEMENTARY NOTES

14. ABSTRACT
This report summarises the application of simultaneous Interferometric Laser Imaging Droplet Sizing (ILIDS) to the spray characterization of a generic double-swirl prefilming model aeroengine atomizer, which injects an annular liquid sheet of 0.5 mm thickness at the nozzle exit, sandwiched between an inner and an outer co-rotating swirling air streams.
Planar spray measurements are obtained using a non-invasive laser-based Interferometric Laser Imaging Droplet Sizing (ILIDS) technique which is capable of providing simultaneous planar measurements of droplet size, velocity and number density in the resulting spray.Experiments are reported for a water spray for different axial (Z) and radial (R) locations for different air and water flow conditions. Apart from time-averaged droplet size and velocity measurements, ILIDS allows unique measurements of other important statistical quantities, including droplet-droplet spatial velocity correlation, which is important for evaluation of new modeling approaches for the droplet fluctuating motion, and is presented here for different separation distances between droplets and conditional on droplet size. In addition the extent of droplet clustering for different droplet size classes is presented and the corresponding cluster dimensions quantified, as estimated from the radial distribution function (RDF) measured conditional on droplet size classes. Finally, measurements of mean and fluctuations of droplet number density for different droplet size classes are reported. The new physical understanding of the spray dynamics and droplet cluster formation in sprays, provided by the novel measured quantities, is discussed.

15. SUBJECT TERMS
AOARD, Combustion, Spray

16. SECURITY CLASSIFICATION OF:			17. LIMITATION OF ABSTRACT	18. NUMBER OF PAGES	19a. NAME OF RESPONSIBLE PERSON
a. REPORT	b. ABSTRACT	c. THIS PAGE			KNOPP, JEREMY
Unclassified	Unclassified	Unclassified	SAR	19	19b. TELEPHONE NUMBER *(Include area code)* 315-227-7006

Standard Form 298 (Rev. 8/98)
Prescribed by ANSI Std. Z39.18

PROGRESS REPORT

AWARD N°: FA2386-13-1-4065

TITLE: Novel techniques for quantification of correlation between primary liquid jet breakup and downstream spray characteristics

INVESTIGATOR: Professor Y. Hardalupas

ORGANISATION: Imperial College of Science, Technology and Medicine

REPORTING PERIOD: From: 18 April 2015
To: 17 April 2016

PROJECT START DATE: 18 April 2013

DATE OF ISSUE OF THIS REPORT: 8 May 2016

ADMINISTRATIVE OFFICE: Asian Office of Aerospace Research and Development (AOARD)

GOVERNMENT PROGRAM MANAGER: Col David Hopper

Table of Contents

List of Symbols, Abbreviations and Acronyms

AMD	Arithmetic Mean Diameter
D	Droplet Diameter
ILIDS	Interferometric Laser Imaging Droplet Sizing
N	Number density of droplets
n	Standard deviation of droplet number density fluctuations
Nd:YAG	Neodymium Yttrium Aluminium Garnet
PDPA	Phase Doppler Particle Analyser
PTV	Particle Tracking Velocimetry
R	Radial distance from spray axis
RDF	Radial Distribution Function
R_{dd}	Spatial correlation coefficient of droplet velocity fluctuations
R_{uu}	Spatial correlation coefficient of axial droplet velocity fluctuations
R_{vv}	Spatial correlation coefficient of radial droplet velocity fluctuations
SMD	Sauter mean diameter
std	Standard Deviation
t	Liquid film thickness
V_a	Area-averaged Air Velocity at the nozzle exit
V_l	Area-averaged Liquid Velocity at the nozzle exit
Z	Axial Distance along the spray axis
ρ_a	Air density
σ_l	Liquid surface tension

List of figures

Summary

This report summarises the application of simultaneous Interferometric Laser Imaging Droplet Sizing (ILIDS) to the spray characterization of a generic double-swirl prefilming model aeroengine atomizer, which injects an annular liquid sheet of 0.5 mm thickness at the nozzle exit, sandwiched between an inner and an outer co-rotating swirling air streams. Planar spray measurements are obtained using a non-invasive laser-based Interferometric Laser Imaging Droplet Sizing (ILIDS) technique[1,2], which is capable of providing simultaneous planar measurements of droplet size, velocity and number density in the resulting spray.

Experiments are reported for a water spray for different axial (Z) and radial (R) locations for different air and water flow conditions. Apart from time-averaged droplet size and velocity measurements, ILIDS allows unique measurements of other important statistical quantities, including droplet-droplet spatial velocity correlation, which is important for evaluation of new modeling approaches for the droplet fluctuating motion, and is presented here for different separation distances between droplets and conditional on droplet size. In addition the extent of droplet clustering for different droplet size classes is presented and the corresponding cluster dimensions quantified, as estimated from the radial distribution function[5] (RDF) measured conditional on droplet size classes. Finally, measurements of mean and fluctuations of droplet number density for different droplet size classes are reported. The new physical understanding of the spray dynamics and droplet cluster formation in sprays, provided by the novel measured quantities, is discussed.

1. Introduction

Several liquid-fuelled combustion systems, such as liquid propellant rocket engines and gas turbines, rely on air-blast atomizers in order to generate appropriate fuel spray characteristics for the combustion process. In general, such fuel injectors are axisymmetric, and, in order to enhance the atomization process, they are designed to form a liquid sheet at the nozzle exit, which is sandwiched between inner and outer air flows. The flame stabilization is often accomplished by introducing swirl to the air streams. In addition to recirculation of the combustion products, swirl is important for enhancing mixing, controlling combustion instability and also, promoting disintegration of the liquid sheet[1], [2], [3]. Considering the challenges in studying spray combustion due to interacting complex physical and chemical processes, idealized sprays are studied to minimize coupling effects between the different processes and to provide parametric results. The present research reports experimental spray characterization of a generic double-swirl prefilming model atomizer, which issues at the nozzle exit a thin annular water sheet sheared between inner and outer co-rotating swirling air streams under ambient conditions. The purpose here is to study the dispersion of the spray and interaction of droplets with gas turbulence that involves physical mechanisms, which are not yet well understood[4]. Specifically, we report the two-point correlation of droplet velocity fluctuations and address the spatial preference in such correlations within the spray with respect to the distance from the nozzle exit and according to droplet size classes. This is important for modeling spray dispersion, especially with Eulerian spray models[5]. In sprays, instantaneous clustering of droplets, defined as regions where the local droplet concentration becomes larger than the mean value, can occur either due to the unsteadiness of the break-up process of a liquid jet/sheet, or due to the interaction of droplets of widely different sizes with the turbulent gas flow[6]. This can result in restricted oxidizer access to evaporating droplets within a cluster leading to the so called ‘group evaporation’, which can have profound effect on flame location and distributions of temperature, fuel vapor and oxygen[7]. In this paper, we report quantitative measurement of droplet clustering in the non-evaporating spray from the air-blast atomizer. However, these quantities necessitate planar measurement of droplet characteristics, in contrast to ‘point’ measurements, for example, by a phase Doppler particle analyser (PDPA). Thus, a planar droplet sizing optical technique, Interferometric Laser Imaging for Droplet sizing or ILIDS, was used in the present study, and its capability is demonstrated for measurement of spatial correlation of droplet velocity and droplet clustering conditional on droplet size for which limited experimental data are available.

2. Experimental set-up

This section describes the details of the atomizer, the instrumentation and the flow and optical arrangements for the experimental characterization of the air-blast spray.

2.1 The atomizer

The design of the prefilming atomizer (as shown in Figure 1a), manufactured at Imperial College, was based on an existing atomizer at ONERA[8]. The liquid entering into the nozzle is allowed to pass through a circular channel, which evenly distributes the liquid in to six metallic tubes, which direct the liquid in to an annular converging passage eventually leading to an annular liquid sheet of thickness (t) of 0.5 mm. The air supply is from the top of the injector. A part of the air flow enters into the inner swirler (diameter 25 mm), while

the other part goes into the outer swirler (external diameter 50 mm). Both swirlers are concentric with a swirl angle of 45°.

Then, the inner and the outer air pass through the respective diffuser sections before exit. To avoid air flow separation near nozzle exit, the inner and outer diffusers are designed to follow spline profiles resulting in smooth expansion of the air flows.

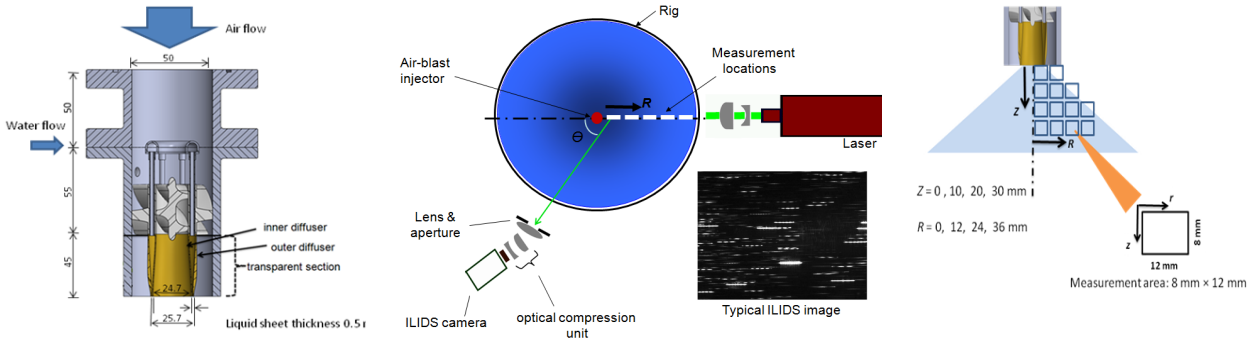

(a) (b) (c)

Figure 1: (a) Schematic of the double swirl air-blast injector. (b) Optical arrangement for the ILIDS technique. (c) The experimental measurement locations in the spray.

2.2 Optical arrangement

Planar measurements of droplet characteristics (size, velocity and number density) is achieved by application of the ILIDS technique[9], [10], which makes use of the interference fringes, formed due to reflected and first order refracted scattered light from individual droplets when imaged by a defocused optical arrangement, to determine the droplet size. The number of fringes present in each of the imaged fringe patterns is proportional to the droplet diameter. The characteristic interferogram is observed at a defocused plane with a far field arrangement of receiving optics through the camera. The defocusing is achieved and controlled by using a pair of cylindrical lenses placed in between the collecting lens and camera[10]. The droplet velocity is measured by tracking position of individual droplets in a pair of ILIDS images captured at a definite time interval. Figure 1b presents the schematics of the experimental arrangement. For measurements by ILIDS, the flow field was illuminated by a frequency-doubled, double-pulse Nd:YAG laser (120 mJ/pulse at 532 nm; beam diameter 5 mm; 5 ns pulse width; New Wave Research). The laser beam was converted to a laser sheet using a series of cylindrical lenses such that the height and thickness of the laser sheet at the measurement location were about 25 mm and 1 mm, respectively. The scattered light from droplets was collected using a CCD camera (PCO; Sensicam QE, 12 bit, 1040 × 1376 pixels^2) via a collecting lens (135-mm f /2.8 Nikon) positioned at a forward scattering angle of θ = 69° with respect to the direction of the laser sheet. A pair of cylindrical lenses, introduced between the objective and the ILIDS camera, optically compresses the fringe pattern for each droplet in the vertical direction only, and generates out-of-focus image on the focal plane. The camera was aligned under the Scheimpflug condition in order to achieve uniform length of fringe patterns. The collecting angle (α), centered on the main angle of camera orientation, was 5.35° for an object distance of 300 mm, resulting in a spatial resolution κ = 6.28 μm/fringe for the ILIDS system. The delay time (ΔT) between the two laser pulses was chosen as a compromise between the accuracy of sub-pixel interpolation and minimizing the probability of droplets moving out of the plane of the laser sheet, and was different for different measurement locations and flow conditions. A typical ILIDS image is shown in Figure 1b. The viewing area at each measurement location was nearly 8 mm × 12 mm. The droplet concentration was measured by counting the number of detected droplets in the ILIDS image, which

corresponds to a volume of 8×12×1 mm^3 in the present case (thickness of the laser sheet ≈ 1 mm). We note here that, in any instantaneous ILIDS image, the validation procedure of the image processing does not reject preferentially some droplet sizes. Thus, the relative droplet number counts of different size classes remain the same compared to the case when all droplets in an image are considered. The details of ILIDS image processing can be found in [11] and [12].

2.3 Flow conditions

The measurements are performed for different axial and radial measurement locations as shown in Figure 1c. The location of any measurement window is specified by R and Z, which are defined respectively from the nozzle exit and nozzle axis up to the beginning of any measurement locations. The experiments are performed for different axial and radial locations, as shown in Figure 1c, for Z = 0, 10, 20, 30 mm, and R = 0, 12, 24, 36 mm. Though, experiments have been performed for different flow conditions, the results are presented for air velocity, V_a = 24 m/s and water velocity, V_l = 0.2 m/s, where V_a and V_l are area-averaged velocities calculated at the nozzle exit. The corresponding Reynolds numbers for air and water flows were 8×10^4 and 1400, respectively.

The Reynolds number was calculated based on hydraulic diameter of the air and water flows. The aerodynamic Weber number of the liquid sheet (defined as $\rho_a (V_a - V_l)^2 t / \sigma_l$) was 40, where t is the liquid sheet thickness.

3. Results and Discussion

3.1 Droplet size and velocity

For the optical settings of the ILIDS technique, the minimum and maximum measurable droplet size (see [11]) are about 14 μm and 240 μm, respectively. Figure 2(a) shows droplet size distribution at three different measurement locations at (Z, R) = (0 mm, 0 mm), (30 mm, 0 mm), and (30 mm, 24 mm). These plots show broad distribution of droplet sizes at the measurement locations, while the small droplets of size 15-40 μm are dominant.

The droplet size distribution is broader away from the nozzle exit and the spray axis, thus the Arithmetic Mean Diameter (AMD) and Sauter Mean diameter (SMD) are higher at these locations. This is depicted in Figure 3, which shows the variation of SMD at different measurement locations. The increase in SMD with axial direction is more prominent close to the nozzle axis, which is attributed to droplet coalescence. For any axial location Z, SMD increases towards the edge of the spray implying large droplets are centrifuged out due to the swirling air flow. Though further away from the spray edge, the SMD decreases slightly. Figure 2(b) shows the correlation between instantaneous droplet size and droplet axial velocity. For measurement locations close to the nozzle axis, the axial velocity is mostly negative (this will be explained later), and, in such case, the axial velocity sharply decreases with droplet size. Further away from the spray axis, the droplet flow is positive and downward, and larger fluctuations of velocity are present for small droplets as observed for location Z = 30 mm and R = 24 mm. Figure 2(c) shows the correlation between droplet axial and radial velocity for droplets of all sizes. It can be observed that the two velocity components are nearly independent of each other close to the spray axis, while the correlation becomes strong and positive close to the spray edge since the radial velocity of droplets increases away from the axis due to droplet centrifuging. In the rest of the text, the results pertaining to statistical quantities are presented for three different droplet size classes of 15-30μm, 30-45μm and 45-60μm. The size width of 15 μm for each

size class was selected as a compromise between higher statistical uncertainty (with smaller width) and obtaining size averaged information (with larger width) with sufficient number of samples.

The stokes number of the droplets based on characteristic time of the large scale turbulent for the three droplet classes were 0.005, 0.01, 0.02 for axial location Z = 0 mm, and 0.02, 0.06, 0.12 for axial location Z = 30 mm. Thus, the droplet response to the gas velocity fluctuations is poorer downstream of the nozzle exit. In general, the statistical uncertainty was higher for larger droplet size class due to reduction of sample size and it is quantified for each measured quantity in the relevant part of the text.

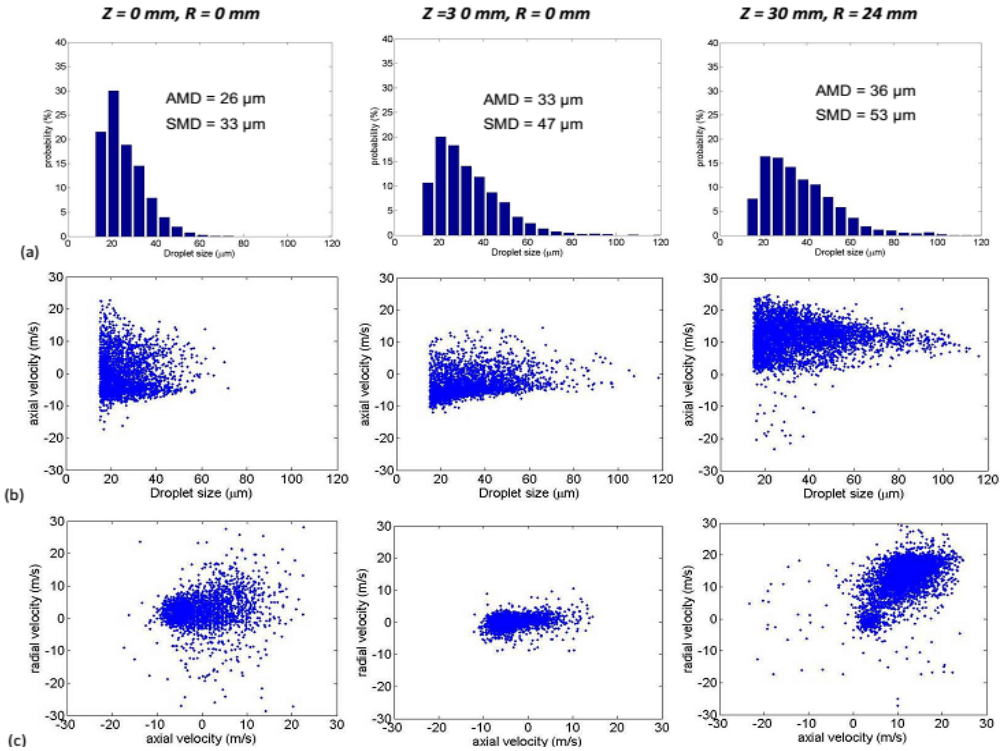

Figure 2: (a) Droplet size distribution, (b) correlation between droplet axial velocity and droplet size, and (c) correlation between droplet axial and radial velocity at different measurement locations.

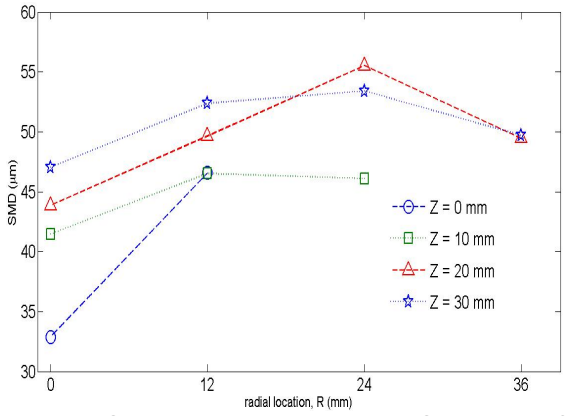

Figure 3: Variation of droplet Sauter Mean Diameter (SMD) at different axial and radial measurement locations.

Figure 4 presents droplet velocity vector plots at different measurement locations for 15-30 µm droplets. Similar trends were observed for droplets of other size classes, and so, not presented here. Since ILIDS uses Particle Tracking Velocimetry (PTV) for calculation of the droplet velocity, the droplet position inside the measurement area was always random.

So, no regular grid could be associated with the instantaneous droplet velocities. Thus, for calculation of the mean velocity, the observed experimental area was divided into regular and square cells of about 2 × 2 mm^2 for droplet size classes of 15–30 μm and 30–45 μm and 3 × 3 mm^2 for droplet size class 45–60 μm. The difference in the averaging area for different size classes was due to the lower probability of detecting larger droplets. The details on the selection of cell sizes can be found in[13]. It can be observed that the droplet flow is axially upward close to the spray axis causing flow reversal, which is due to dominance of an adverse pressure gradient over the axial kinetic energy of droplets away from the nozzle exit. Since small droplets can easily follow the gas flow, Figure 4 can be considered as representative of the gas flow as well. Thus, due to the swirling motion of the air, the, so called, central toroidal recirculation region (CTRZ) exists near the nozzle exit.

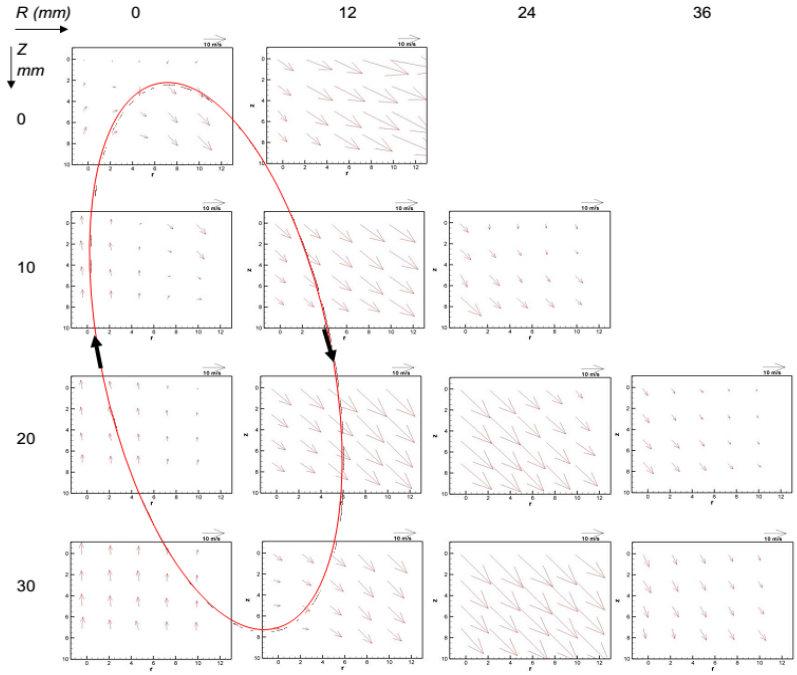

Figure 4: Vector plots of average droplet velocity at different measurement locations for 15-30 μm droplets.

Figures 5 and 6 present average axial and radial droplet velocity for different droplet sizes for different radial locations for measurement stations at Z = 0 mm and 30 mm. The droplet velocity at Figure 5 is plotted for axial locations corresponding to central horizontal line perpendicular to the nozzle axis at each station. The uncertainty in droplet mean velocity with 95% confidence interval was about 20-40%, and higher for larger droplet size class. As mentioned before, the mean axial velocity of droplets is negative close to the spray centre (see Figures 4 & 5). Away from the nozzle axis, the droplet velocity decreases first and then becomes positive and increases and, eventually, reduces till the droplets lose momentum near the edge of the spray. Though, the radial location where the axial velocity is ‘zero’ is larger for locations away from the nozzle. For larger radial distances, the mean radial velocity increases sharply as expected due to the swirling air and becomes the same order as the axial velocity (Figure 6). For the near nozzle location at Z = 0 mm, after the droplet flow again reverses downward, the droplets accelerates following the gas flow. While small droplets follow the gas easily, larger droplets are unable to do so due to their inertia; hence their axial and radial velocity is smaller. Away from the nozzle and close to the spray centre, larger droplets have smaller upward velocity due to inertia effects and larger gravitational influence, while no significant difference between the considered size

classes are observed for other measurement locations. This implies the recirculation zone length varies with droplet size.

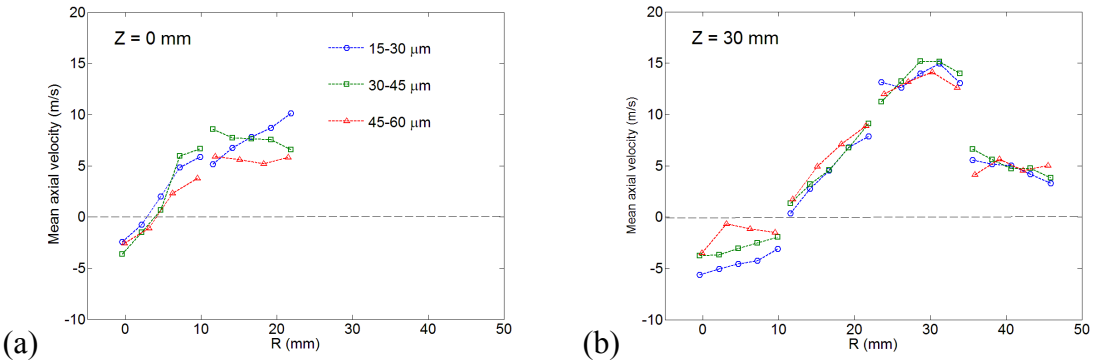

Figure 5: Radial variation of mean axial velocity of droplets of different size classes for axial locations *Z* = (a) 0 mm and (b) 30 mm.

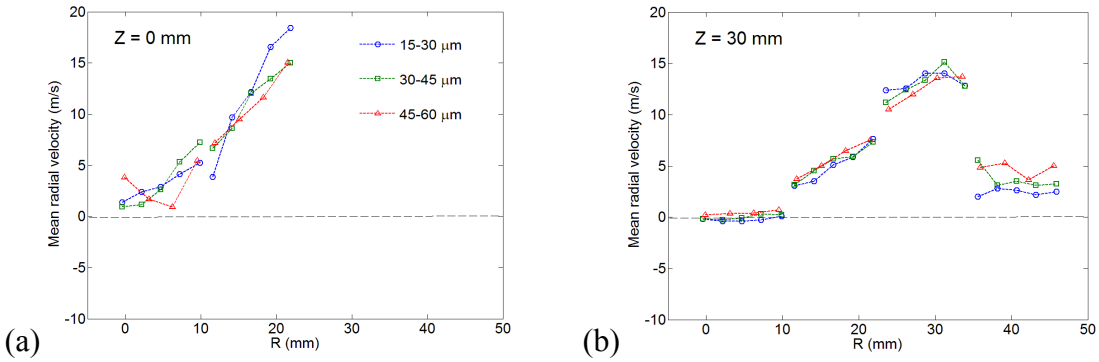

Figure 6: Radial variation of mean radial velocity of droplets of different size classes for axial locations *Z* = (a) 0 mm and (b) 30 mm.

Figures 7 and 8 present the radial variation of standard devia*tions (std) of droplet velocity* fluctuations for different size classes at the two axial locations. Comparing with Figures 5 and 6, it can be discerned that the velocity fluctuations are higher with respect to the mean values close to spray centre, while it is smaller away from the spray axis. The fluctuations of droplet velocity for axial direction are slightly higher than that in the radial direction. Though, no strong dependence on droplet size is observed, the std of axial velocity is consistently higher for the 15-30 μm droplets in comparison to larger droplets.

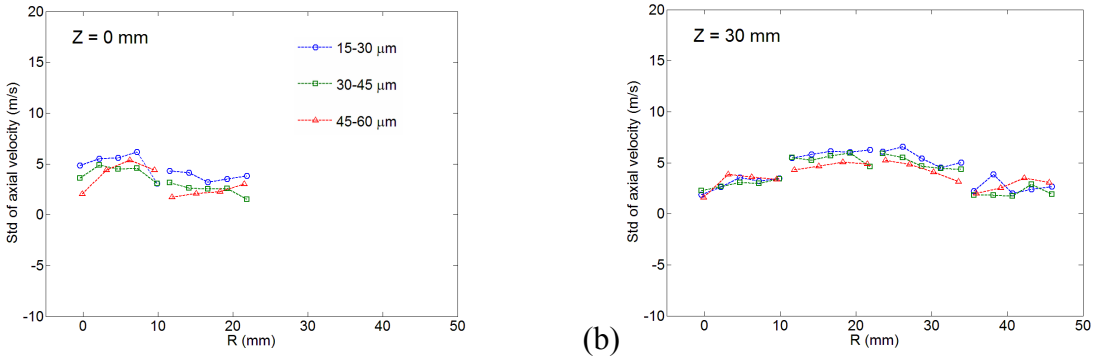

Figure 7: Radial variation of standard deviation (std) of axial velocity of droplets of different size classes for axial locations *Z* = (a) 0 mm and (b) 30 mm.

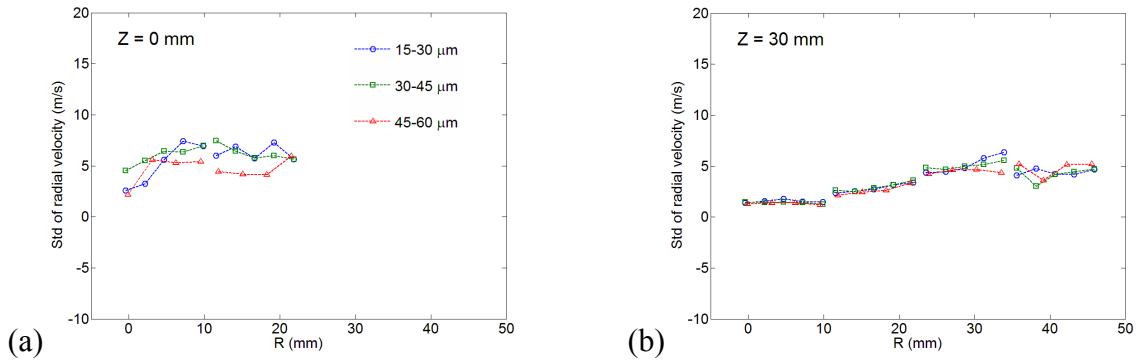

Figure 8: Radial variation of standard deviation (std) of radial velocity of droplets of different size classes for axial locations *Z* = (a) 0 mm and (b) 30 mm.

3.2 Spatial correlation of droplet velocity fluctuations

The two-point spatial correlation of the droplet flow is an important statistical quantity, which provides insight into the two-phase interaction mechanisms and facilitates new approaches for modelling the droplet fluctuating motion[14]. In the context of spray research, such correlations have implication in Eulerian-based spray models that attempt to resolve the spatially variable and time-dependent motion of the droplet phase[5]. Though, measurement of such quantities is rarely reported in the literature because of the difficulty in obtaining simultaneous planar measurements of both droplet size and velocity. Moreover, for a polydispersed spray, the correlation must be obtained conditional on droplet size. The ILIDS technique offers such an opportunity. The method of calculating the two-point spatial correlations of droplet velocity fluctuations from ILIDS measurements is described by Sahu et al.[13] and is briefly mentioned below.

The velocity correlation terms were calculated over the whole viewing area. The process of calculating the two-point spatial correlation coefficient of droplet velocity fluctuations, R_{dd} (D, r), as a function of droplet size class, D, is depicted, in Figure 9. For every image sample, *I*, around each droplet position, *J*, a circle with a given radius, named 'radius of separation', *r*, was defined. For each droplet the correlation between the fluctuating droplet velocity and all of the fluctuating droplet velocities, index *K*, which have been measured inside an annular ring (defined within r ± Δr/2), was calculated. This is done for all droplets belonging to the size class D in that image sample, and then repeated for all image samples, *N*. Then, the average of all calculated correlations was obtained and normalized with the product of the respective rms of fluctuations of droplets to obtain the final correlation coefficient, R_{dd}, for the size class D and for radius of separation r. It should be mentioned here that the mean velocity of droplets and gas used to calculate the fluctuating velocity and, the respective rms velocity (used for normalization) were the area-averaged values. Then, Rdd is calculated for different values of 'r' and for all of the droplet size classes. Also, the correlations were calculated for several combinations of the different velocity components of the droplet velocity and each of the correlations was conditional on different droplet size classes. The choice of r and Δr depends on the droplet number count, which can provide statistical convergence. For instance, larger values are chosen for higher droplet size classes as the corresponding probability of occurrence is lower.

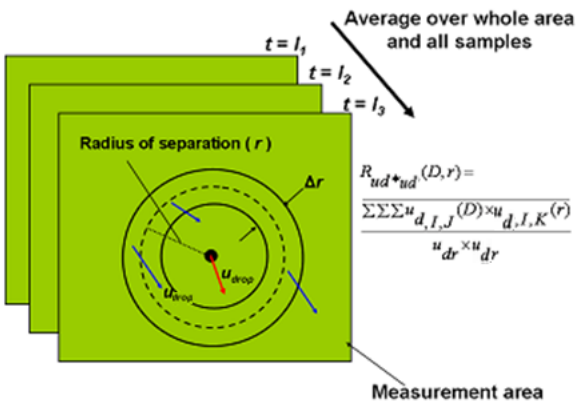

Figure 9: The method of calculation of the spatial correlation of the velocity fluctuations.

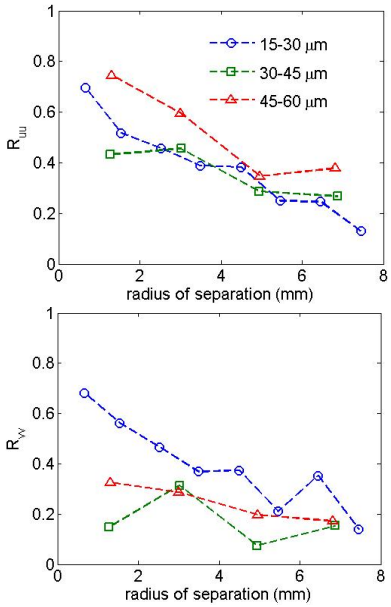

Figure 10: Spatial droplet velocity correlation for (a) axial velocity (R_{uu}) and (b) radial velocity (R_{vv}) for different radius of separation conditional on droplet size classes at *Z* = 30 mm, *R* = 24 mm.

The spatial droplet velocity correlation for axial velocity (R_{uu}) and radial velocity (R_{vv}) are shown in Figure 10 for different droplet size classes for the location Z = 30 mm, R = 24 mm, as an example. The uncertainty in the measured correlation coefficients is about ± 0.1—0.2 depending on the droplet size class considered. The evolution of Ruu for different separation distance indicate that the correlated motion among droplets of a given size class sharply reduces away from a test droplet within the measurement area, and the correlation is slightly better for larger droplets. Since this measurement location is close to the spray edge and away from the nozzle exit, both R_{uu} and R_{vv} are of same order for smaller droplets of 15-30 μm. However, in radial direction, the larger droplets are weakly correlated.

Figure 11 shows the evolution of R_{uu} and R_{vv} for 15-30 μm droplets along the nozzle axis (R = 0 mm) for different Z locations away from the nozzle exit. It can be observed that the droplet flow in the axial direction tends to be better correlated to itself, as the droplets move downward. Also, the slope of the Ruu curve increases implying the increase in length scales of the droplet-droplet correlated motion downstream. Though not shown here, Ruu was found to be lower for larger droplet size classes, however, similar increasing trend in Ruu along the spray axis was observed. The correlation in radial velocity was found to be much smaller ($R_{vv} < R_{uu}$) as can be observed in Figure 11(b) for 15-30 μm droplets. This indicates the strong inter-phase coupling of the droplet flow in axial direction compared to the radial direction. Figures 12(a) and (b) present the radial evolution of R_{uu} and R_{vv} for 15-30 μm droplets away from the spray axis at the axial location Z = 30 mm from the injector exit. Ican be observed that the correlation in droplet axial velocity reduces towards the spray edge, while it increases for the radial velocity component. For larger droplets R_{uu} was smaller for larger droplets, and found to be neatly invariant for different radial locations across the spray, though, Rvv was found to increase away from the spray axis.

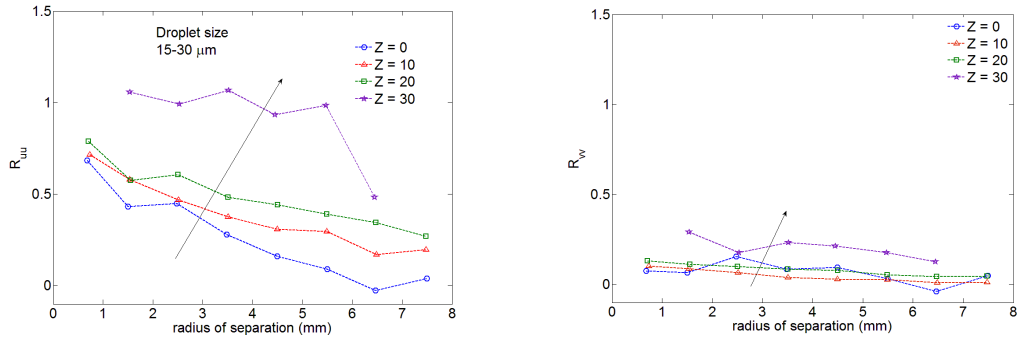

Figure 11: Axial evolution of the spatial droplet velocity correlation for (a) axial velocity (R_{uu}) and (b) radial velocity (R_{vv}) for 15-30 µm droplets for different *Z* locations along the nozzle axis at *R* = 0 mm.

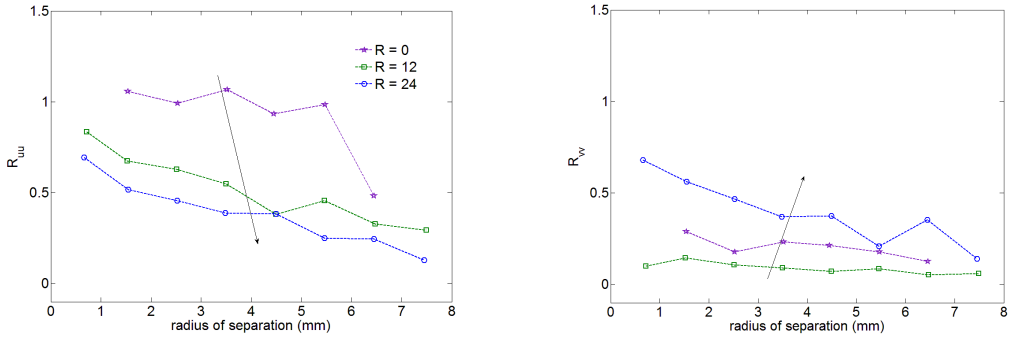

Figure 12: Radial evolution of the spatial droplet velocity correlation for (a) axial velocity (R_{uu}) and (b) radial velocity (R_{vv}) for 15-30 µm droplets for different radial (*R*) locations at the axial location *Z* = 30 mm.

3.3 Measurement of droplet clustering in the spray

Due to wide range of droplet size distribution in sprays, different dynamic behavior of droplet dispersion and interaction with the surrounding gas leads to formation of instantaneous clusters of droplets in the flow[6]. Droplet clustering leads to significant increase of the instantaneous local droplet concentration above the mean value, which causes the inter-droplet spacing to become sufficiently small so that interaction between neighboring droplets prevents the penetration of oxidizer leading to group evaporation of droplets [7]. Figure 13 shows the radial variation of the mean droplet number density (N) and the intensity of droplet number density fluctuations (n/N , n is the std) for different size classes for the near nozzle location (Z = 0 mm) and away from the nozzle (Z = 30 mm). N is normalized with respect to the mean droplet number density at location Z = 0 mm and R = 0 mm. For Z = 30 mm location, the droplet number density first increases away from the spray axis and then reduces towards the spray edge. Similar trend is expected for the near nozzle location, Z = 0 mm, which is though not evident due to size of the measurement window. The intensity of fluctuations of droplet concentration is between 20% and 40%, which signify presence of droplet clusters within the spray. Close to the spray axis, the fluctuations are higher for smaller droplets, though opposite trends are observed for larger radial locations.

The droplet clustering can also be quantified by measuring the radial distribution function (RDF)[15, 16], which essentially measures the probability of finding a second droplet at a given separation distance from a reference droplet compared to a case, where the droplets are homogeneously distributed. It is computed from a field of M droplets by binning the droplet pairs according to their separation distance, and calculating the function:

$$RDF_i = {N_i / \delta V_i} \Big/ {N / \delta V}$$

where N_i is the number of droplet pairs separated by a distance $r_i \pm \delta r/2$, δV_i is the volume of the discrete shell located at r_i , $N = M\,(M-1)/2$ is the total number of pairs and V is the total volume of the system.

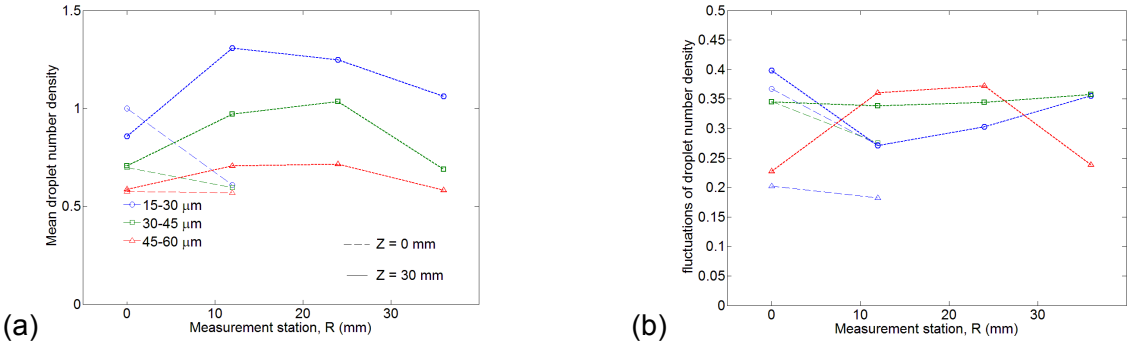

(a) (b)

Figure 13: Radial variation of (a) normalized mean and (b) intensity of fluctuations of droplet number density for different droplet size classes and axial measurement locations at Z = 0 mm and 30 mm.

The ILIDS technique allows measurement of radial distribution function (RDF) conditional on drop size classes, which quantifies the degree and spatial extent of clustering for different droplet size classes and provide the corresponding cluster dimensions. In the present case, the RDF was obtained conditional on drop size classes. Effectively, the value of RDF = 1 means that the droplet distribution is random. For values of RDF>1, this means that droplet clustering occurs. The value of *r,* for which *RDF(r)* becomes larger than 1, provides an estimate of the length scale of the clusters. Figure 14 presents radial evolution of RDF for different droplet size classes at the axial measurement locations Z = 0 mm and 30 mm from the injector exit. It can be observed that at any measurement location and for any radius of separation, RDF increases for larger droplet size classes, so more clustering is evident for 45–60 μm droplets. Also, the length scale of the droplet clusters increases for larger droplets, though this effect is more prominent close to the spray axis. The dimension of the droplet clusters varies between 5 and 7 mm, which is less than the dimensions of the measurement window (≈ 8 mm - 10 mm). From the previous section, it is known that the magnitude of spatial velocity correlations for droplets (R_{uu} and R_{vv}) reduces away from a droplet and attains value close to zero. This indicates that the length scales of the droplet motion influenced by large eddies of the air flow is of the order of the measurement window dimension. Hence, the droplet clustering is expected to be influenced by the large scale motion of the air flow. Since the length scale of the droplet clusters is of the order of spray radius, the large scale eddies of the flow govern formation of clusters of droplets in the spray.

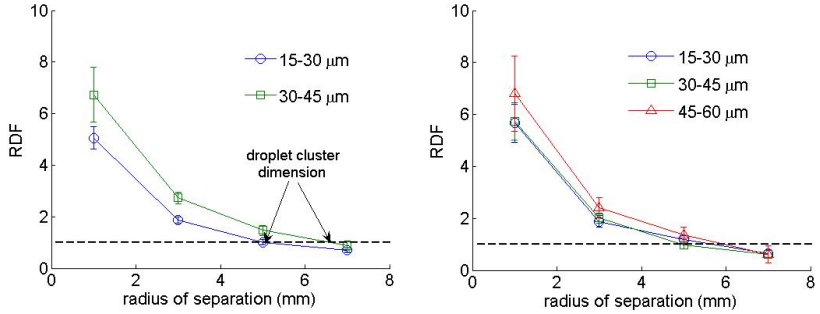

Z = 0mm

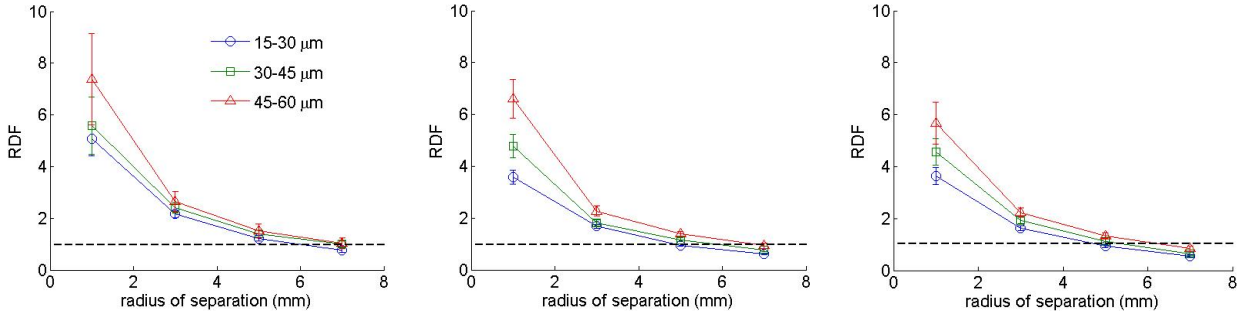

Figure 14: Radial evolution of Radial Distribution Function (RDF) for different droplet size classes at the axial measurement locations Z = 0 mm and 30 mm.

4. Summary and Conclusions

The detailed spray characteristics of a double swirl prefilming air blast atomizer are reported based on planar measurements of droplet size, velocity and number density obtained by applying the ILIDS technique. The increase in SMD of droplets towards the spray edge for both atomizers is explained on the basis of stronger centrifugal force on the larger size droplets due to the swirling flow. The measured mean droplet axial velocity of 15-30 μm size range is negative close to the spray axis and nozzle exit and indicates that the air flow reverses due to the low pressure generated by the swirling air flow.

Apart from the basic droplet velocity statistics for different droplet sizes, the two-point spatial correlation of velocity fluctuations was measured for different separation distances. The spatial correlation for axial velocity fluctuations increases along the spray axis implying larger coherence in droplet motion downstream from the nozzle exit, though it reduces towards the spray edge at any axial location. The spatial correlation for radial velocity fluctuations was low close to spray axis and increases for larger radial distances.

The presence of droplet clustering causes fluctuations of droplet number density. The radial distribution function (RDF) was calculated for different droplet size classes and was found to be larger for larger droplets, indicating their increased affinity for droplet clustering. The dimension of the droplet clusters varied with droplet size and was around 30-40% larger for the larger droplet size range on the spray axis. The dimension of the clusters decreased towards the spray edge.

References

1. *Presser, C., Gupta, A.K., Semerjian, H.G., and Avedisian. C.T., Journal of Propulsion and Power, 10: 631-638 (1994).*
2. *Hardalupas, Y., Taylor, A.M.K.P., Whitelaw, J.H., Proceedings of the Royal Society of London Series A, 428: 129–155 (1990).*
3. *Bulzan, D.L., Journal of Propulsion and Power, 11: 1093-1102 (1995).*
4. *Balachandar, S., Eaton, J.K., Annual Review of Fluid Mechanics, 42: 111–133 (2010).*
5. *Vance, M.W., Squires, K., and Simonin, O., Physics of Fluids, 18:063302 (2006).*
6. *Zimmer, L., Domann, R., Hardalupas, Y. and Ikeda, Y., AIAA Journal, 41:2170–2178 (2003).*
7. *Chiu, H.H. and Liu, T.M., Combustion Science and Technology, 17: 127–142 (1977).*
8. *Giuliani, F., Ph.D. thesis, ONERA, Toulouse, France (2002).*
9. *Glover, A.R., Skippon, S.M., Boyle, R.D., Applied Optics 34:8409–8421 (1995)*
10. *Maeda, M., Kawaguchi, T., Hishida, K., Measurement Science Technology 11:13–18 (2000).*
11. *Sahu, S., PhD thesis, Imperial College London, UK (2011)*
12. *Hardalupas, Y., Sahu, S., Taylor, A.M.K.P., Zarogoulidis, K., Experiments in Fluids, 49:417–434 (2010).*
13. *Sahu, S., Hardalupas, Y., Taylor, A.M.K.P., Journal of Fluid Mechanics, 741:98:138 (2014).*
14. *Fevrier, P., Simonin, O. and Squires, K., Journal of Fluid Mechanics, 533: 1–46 (2005).*
15. *Salazar, J., de Jong, J., Cao, L., Woodward, S., Meng, H. & Collins, L., Journal of Fluid Mechanics, 600:245–256 (2008).*
16. *Sundaram, S. & Collins, L., Journal of Fluid Mechanics, 379:105–143 (1999).*